Coastal Dynamics 2017
Paper No. 161

NUMERICAL MODELLING OF HETEROGENEOUS SEDIMENT TRANSPORT: NEW INSIGHTS FOR PARTICULATE RADIONUCLIDE TRANSPORT AND DEPOSITION

Aurélie Rivier[1,2], Pierre Le Hir[2], Pascal Bailly du Bois[1], Philippe Laguionie[1], and Mehdi Morillon[1]

Abstract

A sediment transport module which solves simultaneously bedload and suspended load is developed, in a context of multiclass sediment transport. Different approaches are used to simulate each transport mode: (i) bedload transport results from divergence of transport capacity and (ii) suspension transport is solved using erosion and settling fluxes associated with advection/diffusion equation. A focus is made on the significance of hiding and exposure processes in case of heterogeneous sediment bed. Their influence is strong on bedload sediment transport, and induces specific trends of sediment sorting in sand dunes. The application to heterogeneous sediment dynamics in the macrotidal area of the Normand Breton Gulf (English Channel), show that hiding and exposure processes enhance the trapping of fine sediments (particles <64 µm, on which radionuclides are likely to adsorb) in locations where coarsest sediments are dominant.

Key words: sediment transport, numerical modelling, hiding, exposure, bedload, suspension

1. Introduction

Upon their discharge into the sea, artificial radionuclides can be adsorbed onto fine-grained suspended particles and trapped in a mixture of heterogeneously sized deposited sediments. It is important to better understand the dynamical behaviour of these trapped particles because they could act as secondary, diffused and delayed sources of dissolved radionuclides to the water column when natural (e.g. storm events) or man-made (e.g. dredging operations) bed erosion occurs (e.g. Black and Buesseler, 2014). These fine-grained particles are obviously present in areas of continuous mud deposition; they are also found within much coarser seabed sediments, in areas at apparent hydrosedimentary equilibrium (mean erosion compensated by deposition and/or no averaged sediment flux gradient; Blanpain, 2009), as the result of trapping processes. This process has been scarcely addressed in hydrodynamical models because hiding processes of fine particles by coarser sediment grains are not systematically implemented in standard sediment transport models.

The aim of this study is to develop a numerical model with sorting capacity able to simulate the behaviour of fine sediments in heterogeneous sediment facies. This is possible thanks to multiclass sediment transport formulation, for both bedload and suspended load, and to the sediment bed discretization, that allows layering process depending on depositing fluxes of the different sediment classes. Hiding and exposure processes will be explicitly implemented using the probabilities of a sediment particle to be hidden or exposed in the bed material (Wu *et al.*, 2000).

The transport module is applied at two different scales in this paper. It is first applied to a small scale test-case in order to test its numerical behaviour and to assess the respective contribution of sediment transport by bedload and by suspension. A focus on the influence of hiding/exposure processes is performed. Then, the multi-class multi-layer hydrosedimentary model is applied to a large scale configuration in the English Channel. The behaviour of fine sediments (<64 µm) is tracked to understand how they could be trapped in heterogeneous sediment mixture.

[1] Institut de Radioprotection et de Sûreté Nucléaire (IRSN), PRP-ENV/SERIS/LRC, 50130 Cherbourg-Octeville, France
[2] Ifremer - Centre de Bretagne, DYNECO/DHYSED, CS 10070, 29280 Plouzané, France

2. Model description

2.1. General setting

Hydrodynamics is calculated using the MARS3D model (Lazure and Dumas, 2008) which solves the momentum equations using finite difference scheme under the Boussinesq and hydrostatic approximations. An Arakawa-C computational grid is used in the horizontal dimensions. The vertical coordinate is a sigma level coordinate. Nested-grids method is available to impose a more accurate forcing along open boundaries. Vertical mixing is solved with the generic length scale formulation (Umlauf and Burchard 2003) using similar parameters for a k-ε turbulence closure as those described in Warner *et al.* (2005). Horizontal viscosity depends on grid spacing and it is expressed following Okubo formulation (1971). MARS3D includes a multi-class multi-layer sediment transport module, described in Le Hir *et al.* (2011), which was developed to model sand/mud mixture dynamics. A specific median diameter, density and type (mud, sand or gravel) is defined for each modelled sediment class. Depending on the mud fraction, a cohesive-like or a sandy behaviour is considered. The module solves advection-diffusion equation in the water column and the bed multi-layer management keeps the sediment class distribution resulting from successive erosion/deposition events and enables consolidation within a bed structure.

In this study, the module is extended to the transport of coarser sands and gravels by adding the bedload process which occurs simultaneously with the suspended transport in the continuity of work performed by Blanpain (2009) and Cugier (2000). Two techniques are associated to model sediment transport: (i) bedload transport results from divergence of transport capacity and (ii) suspension transport is computed by solving an advection-diffusion equation with erosion and deposition rates as source and sink terms. Bedload transport rate is assessed following Wu and Lin (2014) which is similar to Wu *et al.* (2000) under current forcing. This formulation was developed directly for heterogeneous sediment mixture, by opposition with other formulae (e.g. Meyer-Peter Muller, 1948; Van Rijn, 1984; and Ribberink, 1998) which were adapted for heterogeneous after being developed for unimodal sediments. By deploying a video camera close to a coarse sediment interface in the field (Blanpain *et al.*, 2009) in the Normand-Breton Gulf, Blanpain (2009) showed that Wu *et al.* (2000) formulation was the most adapted to represent the motion of different granulometric fractions. Using a DNS (Delft Nile Sampler) in environment composed of sand-gravel particles in the Eastern English Channel, Durafour et al (2015) also showed that predicted fractional bedload fluxes deduced from Wu *et al.* (2000) formulation provided a better agreement with measurements in case of graded sediments than formulations of Meyer-Peter Muller (1948), Van Rijn (1984) and Ribberink (1998).

2.2. Sediment transport module description

The procedure differs according to the cohesiveness of the surficial sediment. This character is tested at the beginning of each time step, for each computing cell at the sediment interface. When the mud fraction exceeds a user-defined value, the sediment is considered as cohesive: no bedload occurs, and all particle classes are mobilized as a whole, in proportion of their own mass fraction. On the opposite, under the critical mud fraction, the sediment is considered as non-cohesive, and each class is transported independently of the other ones, in suspension or as bedload, or both. The rates of erosion or bedload may depend on the local composition of the sediment, for instance to account for hiding and exposure processes. In the case of cohesive surficial sediment, erosion is first computed, then an advection/diffusion equation for suspended sediment is solved and then actual deposition is computed. Finally, a consolidation procedure updates the characteristics of each sediment layer: the whole procedure is described in Le Hir *et al.* (2011). In the case of non-cohesive sediment, the procedure has been changed in order to include bed load processes and the resulting flux divergence. The present paper details this adaptation, and provides examples of application in the case of non-cohesive sediment.

First, the thickness of sediment where grains are likely to be mobilized, either as bedload or resuspension, has to be specified. The so-called *active layer* may vary according to the sediment composition, to the hydraulic forcing intensity and to the presence of bedform. In the present applications, this active layer δ_a is chosen uniform and constant equal to 5 cm, a value between those taken by Villaret *et al.* (2013 - 10 cm) and Reniers *et al.* (2013 -2 cm). If the thickness of the bed surface layer is thinner than δ_a, sediments are removed from the underlying layer to feed the surface layer until its thickness reaches δ_a.

For each class, the quantity of sediment which is likely to leave a cell during a time step dt is the sum of the eroded mass (vertical exchange) and the bedload flux (horizontal exchange) integrated over dt. The bedload flux is computed as the local transport capacity expressed in the center of the cell.

For suspension, an erosion rate E_s (kg.m^{-2}.s^{-1}) is calculated following a pick up function as:

$$E_s(iv) = fr(iv)E_0(iv)\left(\frac{\tau}{\tau_{c(iv)}} - 1\right)^n \quad (1)$$

where *iv* is the number of the class, E_0 (iv) is an erodibility constant (kg.m^{-2}.s^{-1}), τ is the bed shear stress, $\tau_c(iv)$ is the critical shear stress for erosion of class iv, *fr(iv)* is the fraction of sediment class *iv* in the active layer and *n* is chosen 1.5 according to literature (*e.g.* as suggested by Le Hir *et al.*, 2011). E_0 was fitted to get suspended fluxes in agreement with suspended transport rates from Wu and Lin (2014). A value E_0 = 0.0002 kg.m^{-2}.s^{-1} gave satisfactory results for fine and medium sand (cf § 2.3.1).

τ_c is calculated following Wu *et al.* (2014):

$$\tau_c(iv) = \theta c\left(\frac{p_e(iv)}{p_h(iv)}\right)^{-m} d(iv)(\rho - \rho_s) \quad (2)$$

where θ_c is the Shields parameter, p_e and p_h are the exposure and hiding coefficients respectively, *d* is the grain size diameter, ρ and ρ_s are the density of water and sediment respectively and *m* is an empirical parameter. After calibration using laboratory and field data, Wu *et al.*(2014) choose *m*=0.6 and θc= 0.03 whatever the size *d(iv)*. For low concentrated mud fraction in a non-cohesive mixture, τ_c is the lowest critical shear stress of the sand fractions.

The bedload transport capacity is formulated from Wu and Lin (2014). It is adapted for heterogeneous sediments in environments submitted to currents and waves and takes into account hiding and exposure coefficients through the critical shear stress. The current-induced bedload transport rate q_b (m^2.s^{-1}) for the sediment size *d(iv)* is:

$$q_{b(iv)} = 0.0053\left(\frac{\tau}{\tau_{c(iv)}} - 1\right)^{2.2} f(iv)\sqrt{(s-1)g\,d(iv)^3} \quad (3)$$

where $s=\rho_s/\rho$ and g is the gravity constant. The bedload flux is directed as the bed shear stress (and then the bottom flow) and can be projected along the *x* and *y* dimensions of the grid, so that each component determines the neighbouring cell where the sediment is likely to go. This projected bedload reads:

$$q_{bx}(iv) = \frac{q_b(iv)\tau_{bx}}{\|\tau_b\|}, \quad q_{by}(iv) = \frac{q_b(iv)\tau_{by}}{\|\tau_b\|}, \text{ respectively} \quad (4)$$

A slope effect is added to the bedload transport rate, distinguishing the transverse and the flow direction slopes, in the same way as Lesser *et al.*, 2004.

Finally, the total mass of sediments leaving the cell (i,j) during a time step *dt* is:

$$mass_{out}(i,j,iv) = E_s(i,j,iv)\,dx\,dy\,dt + \rho_s q_{bx}(i,j,iv)\,dy\,dt + \rho_s q_{by}(i,j,iv)dx\,dt \quad (5)$$

where *dx* and *dy* are spatial resolution in *x* and *y* directions. This quantity is limited by the mass of sediment available in the active layer.

The quantity of the sediment from class *iv* which enters a cell during *dt* is the sum of the quantity of sediment deposited from suspensions (vertical exchange) and the one carried by bedload from adjacent cells (horizontal exchange). The latter can be splitted into *x* and *y* components coming from neighbouring cells along the respective dimension, in an upward frame: when a flow component comes from one side, the corresponding bed load component is the one computed in the cell that shares this side

The deposition flux for sediment of class *iv* is:

$$D_s(iv) = w_s(iv)C(iv)\left(1 - \frac{\tau}{\tau_{d(iv)}}\right) \text{ for mud}; D_s(iv) = w_s(iv)C(iv) \text{ for sand} \quad (6)$$

where w_s is the settling velocity, C is the near-bed suspended sediment concentration and τ_d is the critical shear stress for deposition. w_s is assessed following Soulsby (1997) for sand and is chosen equal to 1 mm.s^{-1} for mud.

Finally, the mass of the sediment class *iv* getting into the cell (i,j) during *dt* is assessed from this deposition flux and bedload transport rates in the neighbouring cells as:

$$\begin{aligned} mass_{in}(i,j,iv) = {} & D_s(i,j,iv)\,dx\,dy\,dt \\ & +(\max(q_{bx}(i-1,j,iv),0) - \min(q_{bx}(i+1,j,iv),0))\,\rho_s dy\,dt \\ & +\big(\max\big(q_{by}(i,j-1,iv),0\big) - \min\big(q_{by}(i,j+1,iv),0\big)\big)\rho_s\,dx\,dt \end{aligned} \quad (7)$$

The deposition procedure in the seabed remains the same as in Le Hir *et al.* (2011) with a supplementary input mass due to bedload. A new layer is created when the surface layer exceeds 10 cm. This thickness is a compromise between computational coast and respect of sediment layering.

The sediment balance results from the difference between the mass entering a cell (eq. 7) and the one getting out (eq. 5): this balance constitutes an explicit expression of the Exner equation, with an upward formulation of bedload fluxes.

For transport in suspension, the advection/diffusion is generally solved in a 3D frame for mud, and either in depth-averaged (2DH) or 3D frames for sand. In any case, the advection flux of sand is corrected in the lower cell of the water column (or in the whole water column if 2DH computation) assuming a logarithmic velocity profile and a Rouse profile for suspended sediment in the layer (Dufois *et al.*, 2014).

In this study, a particular attention is paid to hiding/exposure coefficients p_h and p_e. and their influence on sediment transport in applications. When hiding/exposure processes are activated, p_h and p_e are assessed for each class *iv* following Wu *et al.* (2014):

$$p_h(iv) = \sum_{j=1}^{N} f_j \frac{dj}{d_{iv}+d_j}; p_e(iv) = \sum_{j=1}^{N} f_j \frac{d_{iv}}{d_{iv}+d_j} \quad (9)$$

p_e=p_h=1 for each class when hiding/exposure processes are not taken into account.

2.3. Sediment transport module validation

The sediment transport module is validated by comparing the equilibrium suspended flux to the suspended-load transport rate proposed by Wu and Lin (2014), and the total flux to experiments conducted by Olivier (2004) on a bimodal sandy sediment in a laboratory flume (20 cm deep). The bed is composed of fine sand (255 µm) and medium sand (600 µm) with the same fraction (50% each), and the depth-averaged velocity is 0.58 m/s. In the model, the water column is divided into 20 layers.

Table 1. Comparison of transport rate by bedload (qb), by suspension (qs) and total (qt) from this model, from empirical formulations of Wu et al (2010) and from experiment (Olivier, 2004).

	q_b(600 µm) (m^2.s^{-1})	q_b(255 µm) (m^2.s^{-1})	q_s(600 µm) (m^2.s^{-1})	q_s(255 µm) (m^2.s^{-1})	q_t(600 µm) (m^2.s^{-1})	q_t(255 µm) (m^2.s^{-1})	q_t(600 µm) /q_t(255 µm)
Model	7.2 10^{-6}	5.0 10^{-6}	4.1 10^{-7}	1.9 10^{-6}	7.6 10^{-6}	6.9 10^{-6}	1.1
Wu *et al.* (2000)	7.2 10^{-6}	5.0 10^{-6}	5.4 10^{-7}	1.7 10^{-6}	7.7 10^{-6}	6.6 10^{-6}	1.2
Experiments Olivier(2004)	Not measured	Not measured	Not measured	Not measured	6.4 10^{-6}	5.0 10^{-6}	1.3

2.3.1. *Respective contribution of each transport mode*

Horizontal fluxes in the model are compared to transport rate from Wu et al (2000) (Tab. 1) to verify their consistency and to validate the choice of the erosion rate E_0. Bed load rates from the model are naturally the same as those expressed by Wu et al (2000). Bedload appears to be higher for medium sand than for fine sand. Bedload transport rate is higher for sediments with a diameter of 600 µm than for sediments with a diameter of 255 µm Modelled suspended transport rates are obtained by integrating horizontal fluxes. They are in the same order of magnitude that suspended transport rates from Wu et al (2000) for both classes of sediments (255 µm and 600µm). Suspended transport rate is higher for fine sand than for

medium sand. The contributions of each transport mode are in agreement with those based on Wu *et al.* (2000) formulations.

2.3.2. *Comparison with experiments*
Only total transport rates are measured during experiments of Olivier (2004). Model results have the same order of magnitude as experimental ones. Also, the modelled total transport rate appears higher for medium sands than for fine ones, as in experiment. The ratio between total transport rates of both classes is a little weaker in modelling.

3. Bed-forms migration

3.1. Configuration

The sediment transport module is tested in an idealised case. The migration of two large bedforms (sand dunes) in a numerical flume (500 m long and 6 m deep) is simulated in 2DV frame. Bathymetric variations create velocity gradients that induce divergence of bedload fluxes in the domain. The bed is initially composed of two size classes with the same fraction (50 % each): fine sand (255 µm) and medium sand (600 µm). Sand density is 2600 kg.m^{-3} and bed porosity is 0.42. The initial bedforms are two Gaussian shaped dunes with an elevation of 2 m and *ca.* 60 m extended (Fig. 1). The bed is divided into 10 layers. The 7 topmost layers are 0.1 m thick, the two following are 0.2 m thick and the deepest layer is 3 m thick. Water column is equally divided into 20 sigma-levels, the horizontal spatial resolution is 2 m and the time step is 0.5s. Hydrodynamics are forced by a sea surface slope (2 cm between the inlet (on the left hand side of Fig. 1) and the outlet (on the right, Fig. 1). This forcing creates a unidirectional current characterized by a depth-averaged velocity of 1.1 m.s^{-1} at the entrance and 1.65 m.s^{-1} above the dune crest. The respective contributions of bedload and suspended load on total sediment transport are investigated, together with the influence of hiding/exposure processes on the bed evolution.

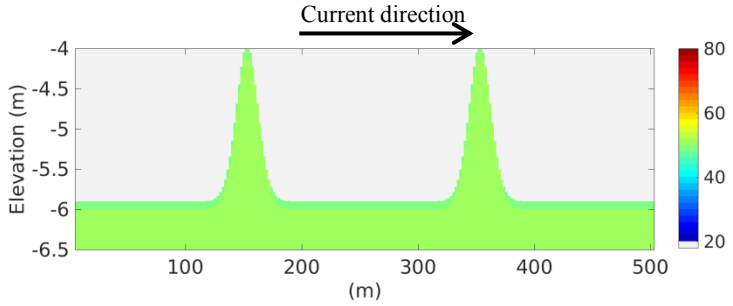

Figure 1. Initial bed elevation and composition (Fraction (%) of the finer sand, 255 µm – see colour scale) in the bedform case.

3.2. Results and discussions

Six scenarios have been simulated (Fig. 2): (a and b) scenarios with bed load transport only, (c and d) scenarios with suspended transport only and (e and f) scenarios with combined bedload and suspended load. All transport mode scenarios are either computed with (b, d and f) or without (a, c and e) hiding/exposure processes. The sand dunes longitudinal profile is presented in Fig.3 after 48 hours evolution. In agreement with differences in bedload and suspended load rates (Tab. 1), the deformation and migration rate are quite different in the different scenarios.

In these simulations, hiding and exposure processes play contrasted roles depending on the scenario. In the case of suspended load only, they appear to have a weak influence on the dune evolution (Fig. 2 c-d): a vertical sorting with coarser particles at the crest is observed in both cases, with weaker differences between the crest and through composition when hiding/exposure processes are accounted for. The main result from suspended transport is a strong sorting process on the lee side of the sand bedform. Fine sand is eroded more easily, transported further and deposited downstream in the trough of the dune.

Medium sand becomes dominant on the dune and especially on its crest, and deposits rapidly on the upper half of the lee side.

Processes are not the same in the bedload alone scenario, and hiding and exposure processes appear to have a strong influence on sediment transport and sorting (Fig. 2 a-b). Two opposite behaviours occur between Fig. 2a and 2b. Sediments are well sorted after 48 h when hiding exposure processes are not accounted for (Fig. 2a). The 255 µm sand fraction decreases from 50% initially to 35 % at the crest of the bedforms. This fraction increases gradually along the downstream slope to reach a maximum at the through with a value of 60 %, larger than the initial fraction. A vertical sorting with an upward coarsening trend is clearly visible. This coarser fraction on the top of the dune seems to be induced by a larger bedload transport rate divergence for 255 µm sand than for 600 µm sand at the crest, and conversely at the through. The vertical sorting has an opposite trend when the hiding/exposure coefficients are calculated following equations 8 (Fig. 2b). The fine sediment fraction becomes greater at the crest of bedforms (60%) than at the through (35%). Here critical bed shear stresses is modified by hiding/exposure coefficients and bedload transport rate divergence for 255 µm sand is now weaker than for 600 µm sand at the crest, and conversely at the through. No matter how the hiding/exposure processes are accounted for, bedforms sink down during the first hours in case of bedload only sediment transport (Fig. 2a-b). This subsidence is weaker when slope effects are not taken into consideration (not shown). The first order upwind scheme used to assess bedload transport rate divergence is numerically diffusive and is likely to enhance this collapse.

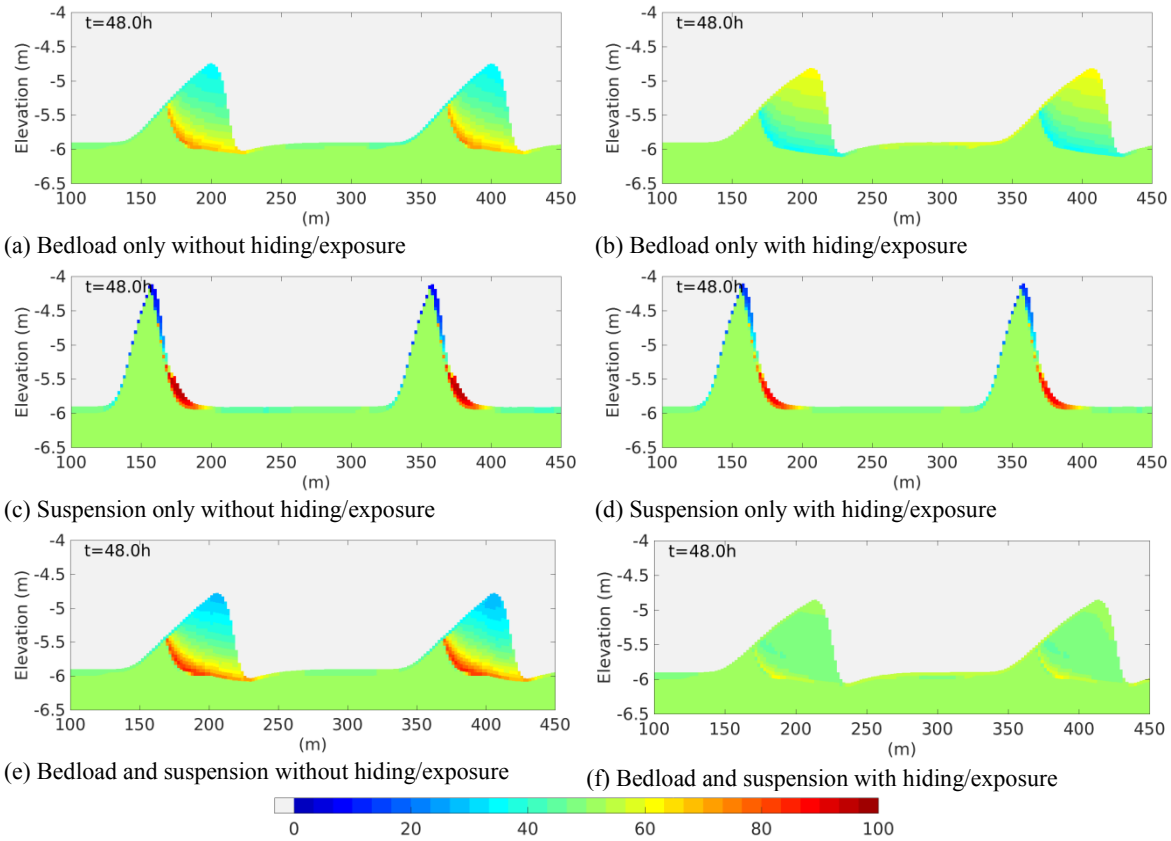

Figure 2. Bed elevation and composition (percentage of finer sand, 255 µm-- see colour scale) after 48h of simulation in case of transport by bedload only (a,b), by suspension only (c,d) and by combination of bedload and suspension (e,f) without (a,c,e) and with (b,d,f) hiding/exposure processes. The grain size of the coarser class is 600 µm.

When transports by bedload and suspension are combined and no hiding exposure are considered (Fig. 2e), the vertical sorting with an upward coarsening trend is exacerbated. The fraction of fine sediment is equal to 30% at the crest and reaches 70 % at the through. This behaviour is expected without hiding/exposure processes: trends are similar for bedload-induced and suspended load induced sorting when no hiding/exposure is considered, and then effects are cumulated. In the case where hiding and

exposure processes are accounted for, the sorting trends were opposite when induced by bedload or suspended transport, so that they compensate when all processes are taken into account, at least with the adopted parameterization. In simulation, sediments are poorly sorted after 48h with hiding/exposure coefficients calculated with equations 8 (Fig. 2f) when sand are transported by bedload and suspension. A weak vertical sorting with upward coarsening trend is observed with a fine sediment fraction of 53 % at the crest and 46% at the through. Olivier (2004) measured small differences of composition between crests and slopes during experiments in a flume with also 2 sediments having the same initial fraction of 50% and grain size diameters of 255 µm and 600 µm. She got a slight downward coarsening trend, with +7.3% fine sand on the crest and -1% fine sand on the trough. Our modelling results are in agreement with this trend only when hiding/exposure are considered, which exhibits the potential importance of these processes. Blom *et al.* (2003), also describe a downward coarsening trend over bedforms, with however coarser sediments and a trimodal mixture. For these sediment sizes, bedload is dominant. These observations from Blom *et al.* (2003) can be qualitatively compared to our bedload only scenarios, and an agreement can be concluded in the case hiding/exposure processes are considered (Fig. 2b). However, other observations on sand dunes show opposite sorting trends, especially in macro-tidal environments (e.g. Stolk 2000), and a definite conclusion may be precocious.

4. Application to English Channel

4.1. Configuration

The regional model MARS 3D is applied to heterogeneous sediment dynamics in the English Channel, between France and United Kingdom, with the new sediment transport module. The area is macro-tidal along the southern coast (France), and experiences very strong current in the narrow central part, which induces marked gradients of sediment composition. One important issue for environmental questions is the fate of fine material and associated contaminants in such a sedimentological context. The model has a 1km horizontal resolution, and considers 10 sigma layers in the water column, with a refinement close to the bottom. The time step is 30 s. The model extends over the whole English Channel (Fig. 3) and is forced by tidal elevation and storm surge at open boundaries, provided by a wider model. First computations were conducted from November 2011 to December 2012, the sediment transport module starting after 10 days of hydrodynamics initialization. Wave action is neglected in the present study.

Six sediment classes (described in Tab. 2) are introduced in the model. For each class the grain density is 2600 kg.m^{-3} and the bed porosity is 0.42. Initially, the bed is equally divided into 10 layers 5 cm thick. Concentrations of each bed sediment class are initialized to fit sediment facies from Larsonneur (1971), following the approach proposed by Bailly du Bois (2000). In this method, granulometric curves associated with each sediment facies were digitalized and parameterized. The initial distribution of the six modelled classes in the bed is obtained from these parameterisations. Fig. 3 (right) shows the initial distribution of fine and medium sized sediments (less than 2 mm) in the Normand-Breton Gulf where a focus is made. Initial concentration in the water column is zero for classes 2 to 6 whereas concentration in the water column for finest sediments (class 1) are initialised from November MODIS monthly climatology of non-algal suspended particulate matter (Gohin, 2011).

Table 2. Characteristics of the sediment classes in the model

Class number (iv)	Grain size	Critical shear stress (without hiding/exposure coefficient) (N.m^{-2})	Settling velocity (m.s^{-1})
1	<64 µm (d=20 µm)	Variable (see § 2.2)	1.0 10^{-3}
2	100 µm	0.046	7.1 10^{-3}
3	200 µm	0.09	0.024
4	500 µm	0.23	0.069
5	2 mm	0.92	0.17
6	20 mm	9.25	0.55

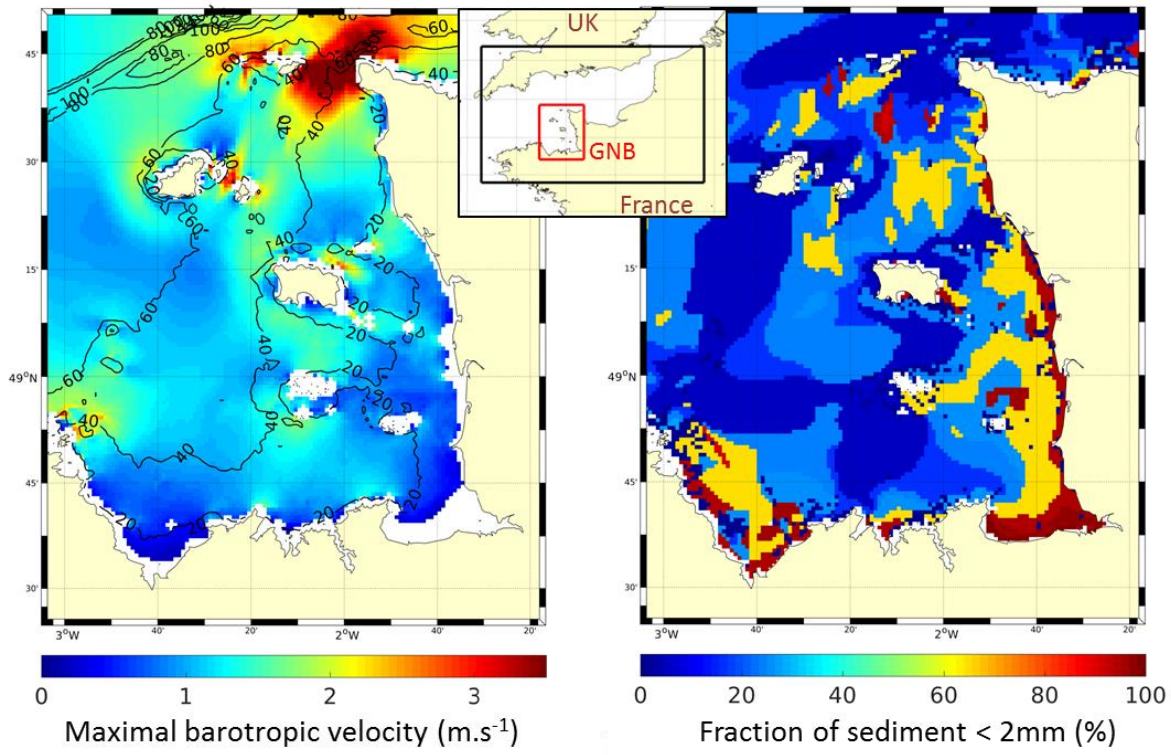

Figure 3. Maximum of barotropic velocity magnitude during a spring tide (left, in colors), bathymetry (left, black line) and fraction of sediment inferior to 2 mm initially in the bed. Calculation domain is located with a black rectangle and studied area with a red rectangle at the top.

The evolution of mud percentage (class 1, d<64 µm) in the < 2 mm sediment fraction is analysed. It is expressed as:

$$P_{mud,inf2mm} = \frac{C(1)}{C(1)+C(2)+C(3)+C(4)} \times 100 \quad (10)$$

where C(iv) is the concentration of sediment class iv in the bed. Dealing with in situ sampling by means of a Shipeck grab, the mud fraction related to sediment classes strictly smaller than 2 mm instead of the bulk sediment is considered as more relevant for analyses, because it prevents inaccuracies due to isolated granules, pebbles and cobbles caught by the grab which could bias the actual sediment class distribution.

4.2. Preliminary results in Normand Breton Gulf

The behaviour of mud is tracked in priority because of its role in radionuclide transport (e.g. ^{137}Cs and ^{60}Co released from AREVA NC reprocessing plant at La Hague) and its capacity to be trapped in a heterogeneous mixture.

Fig. 4 shows the spatial repartition of $P_{mud,inf2mm}$ during a neap tide one year after the start of the simulation. When hiding/exposure processes are not considered, mud is flushed away from the bed to water column within the first time step and deposited only during neap tide (Fig. 4a and 5; red line). $P_{mud,inf2mm}$ is higher and suspended concentration of class 1 (SSC1) lower when hiding and exposure processes occur (Fig. 5; blue line): more finest sediments are trapped. Finest sediment fraction varies mainly with the fortnightly tidal cycle: maximums are observed on neap and minimum on spring. Variation due to semi-diurnal tidal cycle remains weak at this location. Fig. 4b highlights locations where finest particles are mainly trapped during a neap tide. They correspond to areas where bed is composed of coarser sediments (Fig. 3 right), typically where 80 % of sediment is represented by the coarsest class 6. In this case, hiding coefficient is higher and the critical bed shear stress to erode the finer class is larger. Finest sediments which settle at these locations are more difficult to erode in comparison with neighbouring locations. In

these areas of entrapments, $P_{mud,inf2mm}$ is higher in areas where the current intensity is weaker (Fig. 3 rigth), for instance North-North-East of Guernsey and North of Jersey.

$P_{mud,inf2mm}$ is analysed Fig. 6b along the cross section located on Fig. 4b after one year of simulation. $P_{mud,inf2mm}$ is strongly higher between -2.85° E and -2.55° E (Fig. 6b). As previously mentioned, it corresponds to locations where the coarsest fraction is around 80% (Fig. 6a). Finest sediments are more concentrated at -2.6°E than at -2.8°E (Fig. 6a) because of the velocity magnitude which is lower at the eastern part of this spot (Fig. 6c). At -1.9° E, the percentage of coarsest sediment is also around 80% (Fig. 6.a). However, $P_{mud,inf2mm}$ is weak (Fig. 6.b) in comparison with the area between -2.85° and -2.55° E, because the current magnitude remains large locally (Fig. 6.c) and finest sediments can be eroded in spite of a stronger critical shear stress due to hiding processes. The initial size distribution along the cross section was different from the distribution one year later (Fig. 6a), but the distribution after 6 months was similar (not shown), which indicates that a quasi-equilibrium stage has been reached.

Measurements of grain size distributions were made during oceanographic campaigns TRACES 2 014 and TRACES 2015 (Bailly du Bois and Laguionie 2014, Laguionie 2015) in Normand-Breton Gulf. At the studied location in Fig. 5, the fraction of sediments inferior to 64 µm in the fraction of sediments inferior to 2 mm is 10 %. This shows that fine sediment is effectively trapped and not flushed away, even more than in the simulation with hiding and exposure. This discrepancy may come from the bed initialization in the model only by around 1 % of sediments inferior to 64 µm in the fraction of sediments inferior to 2 mm at this location, and from a deficit of suspended sediment input. In our simulation, sediments trapped are mainly sediments initially in suspension which settle after a possible advection and are potentially resuspended partially during spring tide. Suspended sediment concentration (SSC) of class 1 tends to decrease over time in the water column (Fig. 5 bottom), especially without hiding/exposure processes. This is due to the lack of suspended sediments entering at the boundaries. In the Normand Breton Gulf, the part of silts in suspension near the surface coming from the western part of English Channel is high (Rivier, 2013), around 70 % at the studied location. Sediment bed will be in the future initialized sediment distribution more in agreement with *in-situ* measurement, especially for fine sediment fraction.

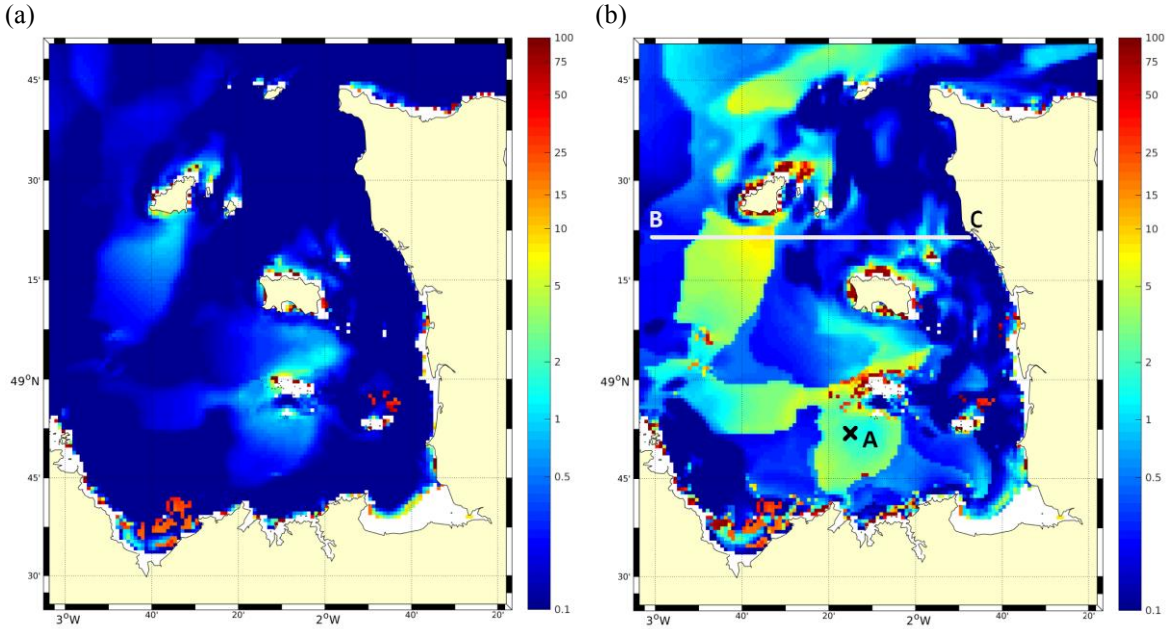

Figure 4. Mud percentage (d<64 µm) in the bed surface (5 upmost centimetres) in the less than 2 mm fraction of sediments (a) without and (b) with hiding/exposure coefficient the 22/11/2012 at 03:00 (after 1 year and 3 days of simulation). The black cross (A) and white line respectively indicate the location of the time-series in Fig.6 and of the section BC analysed in Fig. 6.

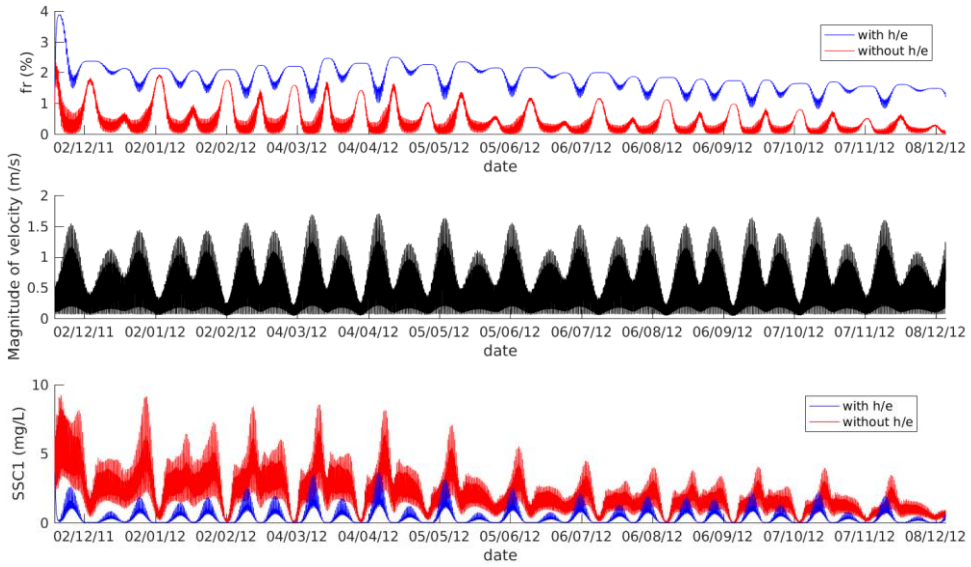

Figure 5. Percentage of mud (d<64 µm) in the bed in the less than 2 mm fraction of sediments without (red) and with (blue) hiding/exposure coefficient (top), magnitude of barotropic velocity (middle) and nearbed suspended sediment concentration (SSC) of class 1 at A (2.25°W, 48.83°N) between 19/11/2011 and 12/12/2012. Location of this point is shown with a cross on Fig. 4.

(a)

(b)

(c)

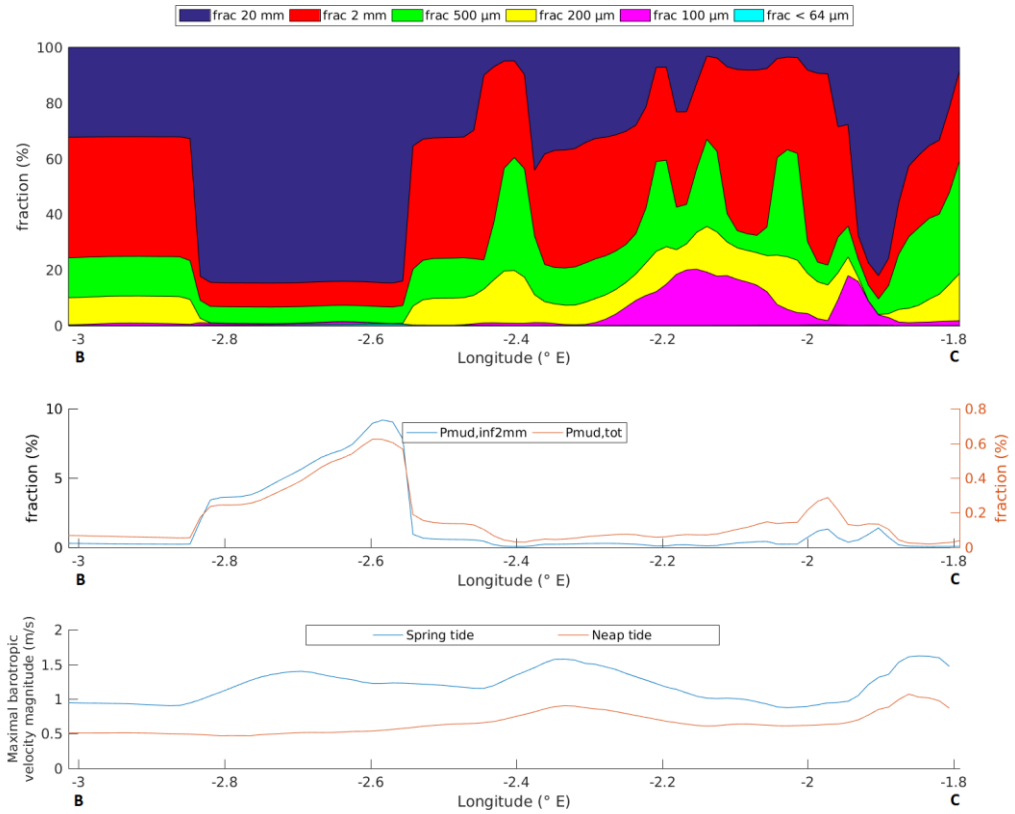

Figure 6. (a) Granulometric distribution, (b) percentage of mud (<64 µm) in the fraction of sediments less than 2mm (blue line) and throughout the sediment (red line), (c) maximal barotropic velocity during a spring tide (blue line) and during a neap tide (red line) along section BC in Fig. 4 (a and b: after 1 year and 3 days of simulation, at 03:00 h on 22/11/2012).

5. Conclusions and Perspectives

The presented results show the strong influences of hiding and exposure processes on sediment transport dynamics in case of multi-classes sediments. They decrease the vertical sorting in case of suspended sediment transport and may reverse it in case of bedload sediment transport. In the studied test-case, sediments are poorly sorted when hiding and exposure are considered, as observed in a flume experiment. In the Normand-Breton Gulf, fine sediments are mainly trapped in areas where gravels are dominant, thanks to hiding processes. Therefore hiding/exposure processes enhance the gradients of fine particle concentrations in the bed, although their role is to attenuate the contrasts in sediment behaviour.

Results presented in this paper are the first steps of this study. Parameters for suspended sediment transport will be refined in order to reproduce observed suspended concentration. The initial size distribution in the bed is crucial. It will be improved in the Normand-Breton Gulf with the recent measurements made during campaigns TRACES 2014 and TRACES 2015 (Bailly du Bois and Laguionie 2014, Laguionie 2015). Moreover the process of fine particles infiltration in a coarser sediment mixture is being implemented in the model. Waves also have a strong impact on sediment dynamics in English Channel, especially in the Western area and Normand Breton Gulf (Rivier et al, 2012), and will be accounted for in the shear stress computation. The ultimate goal of this work is to better account for and to predict the transport and deposition of particle bound radionuclides such as ^{60}Co, ^{137}Cs or transuranics.

Acknowledgements

This work has been achieved thanks to the French State financial support managed by the Agence Nationale de la Recherche, allocated in the “Investissements d’Avenir” framework program under reference ANR-11-RSNR-0002. Numerical simulations were performed with the computer facilities CAPARMOR (CAlcul PARallèlle Mutualisé pour l’Océanographie et la Recherche) from IFREMER.

References

Bailly du Bois, P. and Laguionie, P., 2014. TRACES cruise, RV Côtes De La Manche, http://dx.doi.org/10.17600/14010300 .

Bailly du Bois P., 2000. *Représentation continue des classes granulométriques des sediments superficiels de la Manche à partir des travaux de C. Larsonneur, 1971.* IPSN/DRPE/SERNAT, 13.

Black, E.E. and Buesseler, K.O., 2014. Spatial variability and the fate of cesium in coastal sediments near Fukushima, *Japan. Biogeosciences*, 11: 5123-5137.

Blanpain, O., 2009. *Dynamique sédimentaire multiclasse: de l'étude des processus à la modélisation en Manche*, Doctoral dissertation, Université de Rouen.

Blanpain, O., Bailly du Bois, P., Cugier, P., Lafite, R., Lunven, M., Dupont, J., & Pichavant, P., 2009. Dynamic sediment profile imaging (DySPI): a new field method for the study of dynamic processes at the sediment-water interface. *Limnology and Oceanography: Methods*, *7*(1), 8-20.

Blom, A., Ribberink, J. S., & de Vriend, H. J., 2003. Vertical sorting in bed forms: Flume experiments with a natural and a trimodal sediment mixture. *Water Resources Research*, 39(2).

Cugier, P., 2000. *Développement d'un modèle numérique multicouche hétérométrique pour la simulation du transport sédimentaire en Manche*; caractérisation des principaux processus. IPSN/DPRE/SERNAT/LERFA, 2000-24, 98 p

Dufois F., Verney R., Le Hir P., Dumas F., Charmasson S., 2014. Impact of winter storms on sediment erosion in the Rhone River prodelta and fate of sediment in the Gulf of Lions (NorthWestern Mediterranean Sea). *Cont. Shelf Res.*, 72, 57-72

Durafour, M., Jarno, A., Le Bot, S., Lafite, R., & Marin, F., 2015. Bedload transport for heterogeneous sediments. *Environmental Fluid Mechanics*, *15*(4), 731-751.

Gohin F., 2011. Annual cycles of chlorophyll-a, non-algal suspended particulate matter, and turbidity observed from space and in-situ in coastal waters . *Ocean Science* , 7(5), 705-732

Larsonneur, C., 1971. *Manche centrale et baie de Seine. Géologie du substra tum et des dépôts meubles*. 394 pp, Doctoral dissertation, Université de Caen.

Lazure, P., Dumas, F., 2008. External–internal mode coupling for a 3D hydrodynamical model for applications at regional scale (MARS). *Adv Water Resour* 31(2):233–250.

Laguionie P., 2015. TRACES 2015 cruise, RV Côtes De La Manche, http://dx.doi.org/10.17600/15011900.

Le Hir, P., Cayocca, F. and Waeles, B., 2011. Dynamics of sand and mud mixtures: a multiprocess-based modelling strategy. *Cont Shelf Res*, 31(10):S135—S149.

Lesser, G. R., Roelvink, J. A., Van Kester, J. A. T. M., & Stelling, G. S. (2004). Development and validation of a three-dimensional morphological model. *Coastal engineering*, *51*(8), 883-915.

Meyer-Peter E, Müller R, 1948. Formulas for bed-load transport. *In: Proceedings of the 2nd Congress rivers, International Association for Hydraulic Research, Rotterdam,* pp 39–64

Okubo, A., 1971. Oceanic diffusion diagrams. *In Deep sea research and oceanographic abstracts* (Vol. 18, No. 8, pp. 789-802). Elsevier.

Olivier, C., 2004. *Développement d'un modèle numérique multicouche hétérométrique pour la simulation du transport sédimentaire en Manche ; détermination de l'équation de transport par des mesures en canal de laboratoire*. Rapport DEI/SECRE n° 2004-2.

Reniers, A. J. H. M., Gallagher, E. L., MacMahan, J. H., Brown, J. A., Rooijen, A. A., Thiel de Vries, J. S. M., & Prooijen, B. C., 2013. Observations and modeling of steep beach grain size variability. *Journal of Geophysical Research: Oceans*, 118(2), 577-591.

Ribberink JS (1998) Bed-load transport for steady flows and unsteady oscillatory flows. *Coast Eng* 34:59–82

Rivier, A., Gohin, F., Bryère, P., Petus, C., Guillou, N., & Chapalain, G. (2012). Observed vs. predicted variability in non-algal suspended particulate matter concentration in the English Channel in relation to tides and waves. *Geo-Marine Letters*, *32*(2), 139-151.

Rivier, A. (2013). *Dynamique des matières en suspension minérales des eaux de surface de la Manche observée par satellite et modélisée numériquement* (Doctoral dissertation, Université de Bretagne occidentale-Brest).

Soulsby, R., 1997. *Dynamics of marine sands: a manual for practical applications*. Thomas Telford.

Stolk, A. (2000, March). Variation of sedimentary structures and grainsize over sandwaves. In *Marine Sandwave Dynamics, International Workshop, Université de Lille* (Vol. 1, pp. 23-24).

Umlauf, L., & Burchard, H., 2003. A generic length-scale equation for geophysical turbulence models. *Journal of Marine Research,* 61(2), 235-265.

Van Rijn LC (1984) Sediment transport, part I: Bed load transport. *ASCE J Hydraul Eng* 110:1431–1456.

Villaret, C., Hervouet, J. M., Kopmann, R., Merkel, U., & Davies, A. G., 2013. Morphodynamic modeling using the Telemac finite-element system. *Computers & Geosciences*, 53, 105-113.

Warner, J. C., Sherwood, C. R., Arango, H. G., & Signell, R. P., 2005. Performance of four turbulence closure models implemented using a generic length scale method. *Ocean Modelling*, 8(1), 81-113.

Wu, W., Wang, S. S., & Jia, Y. (2000). Nonuniform sediment transport in alluvial rivers. *Journal of hydraulic research*, *38*(6), 427-434.

Wu, W. and Lin, Q., 2014. Nonuniform sediment transport under non-breaking waves and currents. *Coastal Engineering*, 90, 1-11.